IEEE Access
Multidisciplinary ⋮ Rapid Review ⋮ Open Access Journal

Received June 23, 2020, accepted July 12, 2020, date of publication July 20, 2020, date of current version August 14, 2020.

Digital Object Identifier 10.1109/ACCESS.2020.3010276

Coordinated Control of Electric Vehicles and Renewable Energy Sources for Frequency Regulation in Microgrids

PHOOMPAT JAMPEETHONG, (Member, IEEE), AND SURIN KHOMFOI, (Senior Member, IEEE)
Faculty of Engineering, King Mongkut's Institute of Technology Ladkrabang, Bangkok 10520, Thailand
Corresponding author: Phoompat Jampeethong (60601177@kmitl.ac.th)

ABSTRACT A Control technique of electric vehicles (EVs) cooperating with ac microgrids is considered as an important role with integration of renewable energy sources (RES), i.e. wind and solar farms. As known, the intermittent power generations of these RESs can provide significant changes of the frequency in microgrids. Consequently, outputs of these generations are regarded as continuous disturbances. Previously, the ability to permit frequency stabilizing effect was usually neglected in microgrid design; thereupon, the performance of controller may be ineffective to regulate the frequency in such a microgrid. To address this problem, a new coordination of EV, wind farm (WF), and photovoltaic (PV) for microgrid frequency regulation is proposed in this article. In the control design, the proposed adaptive PI controller is developed by using practical proportional integral (PI) controllers. An effect of a small delay is also considered in input-output pairs of the adaptive PI controllers. Simulation model is developed for validating the proposed controller. Simulation results demonstrate that the proposed coordinated control technique of EVs, WF, and PV power generation provides a better frequency regulation performance than a fixed PI controller under various uncertainties such as wind and solar power fluctuations, *N*-1 outages, disconnection of RESs, load variations, and the number of EVs.

INDEX TERMS Coordinated control, electric vehicle, frequency control, microgrid, renewable energy.

I. INTRODUCTION

Energy management and the environmental crisis are challenging problems in electrical power systems, especially in modern microgrids, because of the restriction of conventional generators and uncertain load demands [1]–[3]. Also, renewable energy sources (i.e., wind farms (WFs) and photovoltaic generation (PVs)) and electric vehicles (EVs) have increasingly been participating in microgrids for generating electrical power [4], [5]. Their high penetration level will provide power support in microgrids [6]. Thereupon, uncertainties from WFs, PVs, and EVs can affect the ability to synchronize loads and generators [7]: these problems restrict from the system inertia being reduced by replacement with such uncertain sources. Moreover, the interaction of electronic-based devices will degrade frequency stability and will eventually lead to system instability without proper control action [8]. Therefore, in the mentioned microgrids, a proper coordinated control strategy from WF, PV and EV sources should be applied to address this problem.

In recent years, several methods and concepts have been proposed to suppress frequency fluctuation in microgrids. In [9], the impact of communication delays on secondary frequency control in a microgrid has been thoroughly investigated. The effect of communication delay is obviously shown to be harmful in secondary frequency control; so, a gain scheduling approach is applied to compensate for the effect of the communication delay. A robust H_∞ and μ-synthesis control strategy to regulate frequency in the microgrid have been proposed in [10]. The method proposed in [10] considers structured and parametric uncertainties in the control design: the results demonstrate that μ-synthesis control provides better performance than H_∞ control. However, in the microgrid configuration in [9], [10] did not address the uncertainty effects from renewable generation. In addition, Tustin's technique based on digital decentralized load frequency control in a microgrid including WFs has been proposed in [11]. The decentralized

The associate editor coordinating the review of this manuscript and approving it for publication was Fabio Massaro.

proportional–integral–derivative (PID) controller is optimized by using a particle swam algorithm. Moreover, communication time delay is also considered in the control loop. Comparing to the analog model, the digital control model performs superior frequency control in terms of reliable performance and satisfactory effective control as discussed in [11]. A cooperative frequency and voltage control method for low-voltage islanded microgrids based on distributed cooperative control has been discussed in [12]. The simulation study in [12] shows that the proposed method could restore frequency under droop-based optimal active power control. An adaptive event-triggered load frequency control has been proposed in [13]. The proposed method in [13] is applied to interconnected microgrids. The results show that large frequency deviation can occur by unbalanced power and time delay. Doubly-fed induction generator (DFIG) control for frequency regulation in a microgrid has been presented in [14]. Simulation results indicate that the DFIG control can provide a fast response to frequency control and consequently contribute to the reduction of frequency deviation. This work also illustrates that the DFIG converter provides faster response than that of conventional plants, i.e., thermal and hydro power plants. However, the study in [14] discusses that wind power uncertainty may have a negative impact on frequency stability. H_∞ robust virtual inertia control of a microgrid with high penetration of renewable energy has been presented in [7]. The study shows that a system inertia is decreased by high penetration of renewable energy owing to its adverse effect on frequency stability [15]. A new application of a robust virtual inertia controller equipped with an energy storage system has been presented in an islanded microgrid with wind and solar farm sources [15]. TThe coefficient diagram method is used to control the virtual inertia. The results, compared with that of the method in [7], demonstrate that the proposed method in [15] provides a better stabilizing effect in terms of frequency regulation. As can be seen, majority of proposed controllers in [11]–[15] are designed in a specific microgrid operation and may not function well in other microgrid operations. Thus far, a few researches have been discussed a coordinated controller in a microgrid including EVs.

Moreover, load frequency control (LFC) in hybrid systems (comprising of WFs, PVs, EVs diesel generator, etc.) has been proposed in [16], [17]. Several optimization techniques have been applied to optimally tune the control parameters of PID controller; for instance, particle swarm optimization (PSO), improved PSO [16], firefly algorithm [16], butterfly optimization (BO) [18], water cycle algorithm (WCA) [16], yellow saddle goatfish algorithm (YSGA) [19], mine blast algorithm (MBA) [17]. It has been reported that the non-integer fractional-order proportional-integral-derivative (FOPID), optimally tuned with WCA, can withstand the change synchronizing coefficient, loading condition, and frequency bias [16]. By using MBA based 2 degree of freedom PID [17], the results have demonstrated that the proposed controller can reduce adverse effects of uncertainties form WFs and PVs; By using BO-based PFOID [18], the results have established the superiority of the BOA-based PFOID controllers under different operating points in terms of frequency fluctuation, tie-line power; By using YSGA-optimized dual-stage PIFOD-one plus PI (PIFOD-(1 + PI)) [19], the results have shown that the proposed YSGA-optimized PIFOD-(1 + PI) can resist variations of wind turbine and system parameters. More comprehensive literature of different controllers utilized in hybrid systems for LFC can be found in [20]. However, in the mentioned of previous works, 1) impact of a small delay in control loops was not considered, 2) optimal fixed control parameters were used for PID controller design. Accordingly, the previous PIDs may not resist the nonlinearity in practical systems.

A coordinated control applying for EVs and renewable energy sources in a microgrid with continuous disturbances is developed in this research to overcome mentioned problems. In the control design, an adaptive PI controller incorporating with a small delay consideration in the control loop are used to regulate frequency at various operating points. The main contributions of this work are listed as follows:

i) The control system is highly robust against various operations, uncertainties, and continuous disturbances,
ii) Coordinated control of EVs and renewable energy sources for stabilizing frequency in a microgrid is achieved,
iii) A small variable time delay in the proposed adaptive PI controller is considered,
iv) A new algorithm, which can automatically change control parameters for frequency stability in a microgrid under various operations, is also developed.

II. CONTROL OVERVIEW

The proposed coordinated control of EVs and wind and solar PV generation in a microgrid is illustrated in Fig. 1. As can be seen, the diagram mainly consists of a group of EVs, solar PVs, and WFs, for supplying load demand. In this study, load, number of EVs, PV and WF power output are assumed to be varied. As a result of these variations, there are significant change of power generation in the total of frequency of the microgrid. To address this problem, frequencies of EV, PV, and WF buses and loads are observed by using data analysis and detection to ascertain the frequency deviation. When the frequency deviation falls into the unacceptable range, the centralized controller is activated to regulate and maintain the frequency within the acceptable range. An energy storage system is connected to the same bus as the EVs to manage the EV power output. However, the PV and WF converters are modulated to control power output of such renewable energy generation. As a result, such control action can regulate the frequency deviation in the microgrid. In this article, the use of a practical PI controller structure will be implemented which is modeled as an adaptive controller so that it can be operated under various uncertainties and disturbances. Moreover, the impact of a small delay is regarded in the control loop.

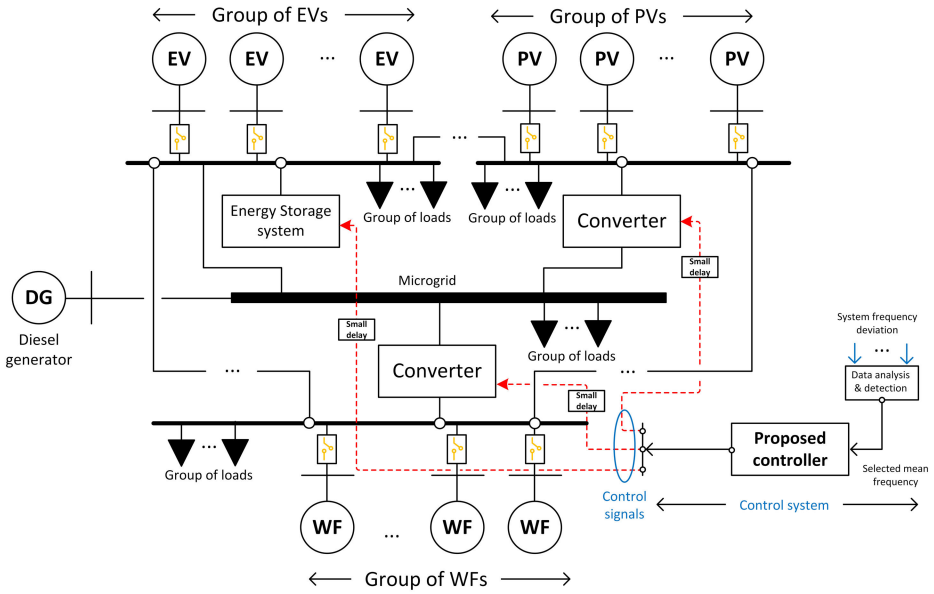

FIGURE 1. Control overview.

The adaptive PI controller will be clearly explained in the next section.

III. MICROGRID MODELING

In this section, the models of the EVs, PVs, WFs and the adaptive controller are created. To begin with, a microgrid state equation will be formulated; then, the control design problem can be obtained.

A. TEST MICROGRID SYSTEM

enerally, frequency stability concerns keeping an equilibrium between loads and generation [21]. Unbalance between load consumptions and power generation in a microgrid with RES always occurs. As a result, it is crucial that a suitable controller strategy should be carefully conducted. Here, the studied microgrid system consisting of EVs, PVs, and WFs is demonstrated in Fig. 2. The relationship among power generation, load demand, system inertia, damping coefficient, and frequency deviation is generally defined by the swing equation as demonstrated in [22],

$$\sum_{i=1}^{N_G}(\Delta P_{m,i}) - \sum_{l=1}^{N_l}(\Delta P_{L,l}) = 2Hs\sum_{i=1}^{N_G}(\Delta F) + D\sum_{i=1}^{N_G}(\Delta F), \tag{1}$$

where ΔF is the frequency deviation; ΔP_m is the change of total generation from EVs, PVs, and WFs; ΔP_L is the change in load power demands; H is the system inertia, and D is the damping factor. Assuming that there is a very small inertia in EVs, PVs, and WFs that can be ignored; then, the relationship between the inertia of the synchronous generator and the microgrid can be determined as clearly explained in [7], [8].

$$H = \frac{\sum_{i=1}^{N_G}(H_{G,i} \cdot S_{G,i})}{S_{MG}}, \tag{2}$$

where N_G is a total number of generators, $S_{G,i}$ and $H_{G,i}$ are the rated power and inertia of the i^{th} generator, respectively. S_{MG} is the rated microgrid power. If we focus on inertia response, the stored inertia power (i.e., kinetic energy) in the rotors of the synchronous generators will counteract the imbalance through the inertia control until before the primary control is used. Additionally, the frequency deviation can be eliminated by controlling the injecting powers of EVs, PVs, and WFs via converters. To robustly maintain the frequency at a nominal value (50±0.5 or 60±0.6 Hz) under various microgrid operations, two control strategies are mainly employed: primary (droop) control and converter control as shown in Fig. 2.

Next, a small variable delay can be formulated as studied in [23],

$$\tau = \bar{\tau} \pm \Delta\tilde{\tau}, \tag{3}$$

where τ, $\bar{\tau}$, and $\Delta\tilde{\tau}$ are the variable time delay, mean value, and variable parts of the variable time delay, respectively. In the frequency domain, equation (3) can be approximated by the first-order Padé approximation [24],

$$e^{\tau s} = \frac{1-\tau s}{1+\tau s}, \tag{4}$$

where e is the natural exponential constant, $s = j\omega_0$ is the complex plane, $j = \sqrt{-1}$ is the complex value, and ω_0 is the natural frequency in rad/s. Substituting (3) into (4), we can get

$$e^{(\bar{\tau}\pm\Delta\tilde{\tau})s} = \frac{1-(\bar{\tau}\pm\Delta\tilde{\tau})s}{1+(\bar{\tau}\pm\Delta\tilde{\tau})s}. \tag{5}$$

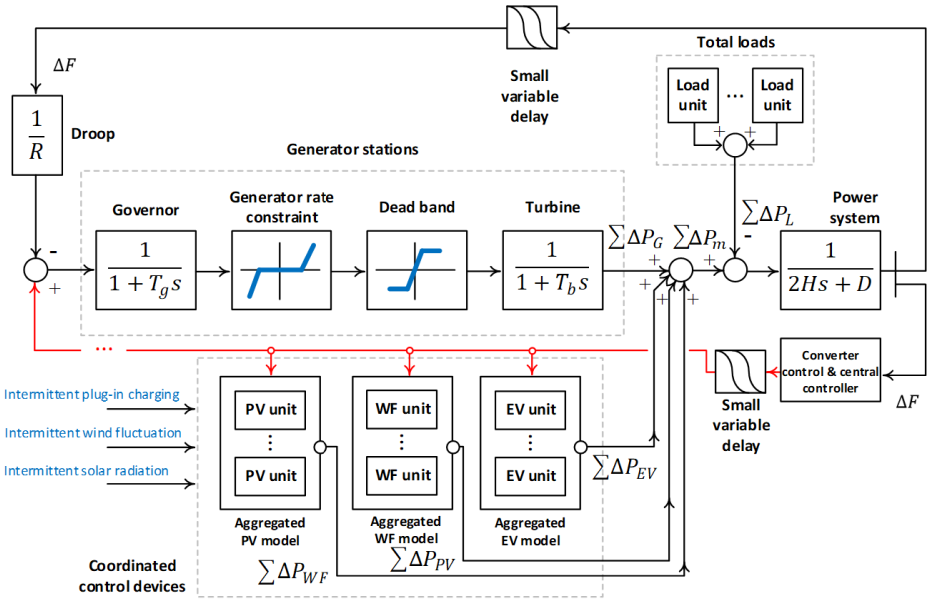

FIGURE 2. Proposed coordinated microgrid control strategy.

Then, at an operating point, the variable time delay can be assumed to be constant as shown in (6).

$$e^{(\bar{\tau}\pm\Delta\tilde{\tau})s} = c_{\bar{\tau}} + c_{\tilde{\tau}}, \tag{6}$$

where $c_{\bar{\tau}}$ and $c_{\tilde{\tau}}$ are constant values at an operation. It should be noted that, although a small delay occurs in control loops, the variable part will cause a malfunction of the control system. As a result, equations (5) and (6) should be considered in microgrid control strategies.

Recently, the synchronous generators in microgrids have been replaced by inverter/converter based RESs. Hence, the response of system inertia (H) and system damping (D), typically during $1-10$ s, is significantly decreased. Accordingly, the rate of change of frequency (derivative of frequency, $\frac{dF}{dt}$) of the microgrids increases, leading to rapid frequency deviation, larger frequency drop and dip, system instability, and, in the worst case, a rapidly cascading failure or power blackout. It should be noted that, during the short time interval of $1-10$ s, the primary control loop may not be effective enough to counteract the contingency, especially under the severe situations of low system inertia caused by renewable energy sources. EV, PV, and WF modeling charts are given in Figs. 3(a), 3(b), and 3(c), respectively. For the EV in Fig. 3(a), the signal from the controller is sent to the energy storage system to charge or discharge power from the EVs. For the PV and WF in Figs. 3(b) and 3(c), the signal from the controller is added to the PWM controller and the current setpoint controller of the PV and WF to modulate the signal in the converter. As a result, the frequency can be regulated.

B. CONTINUOUS DISTURBANCE MODELING

In this article, the continuous disturbance from uncertain modeling (i.e., PV and WF) is given by sum of sine and square

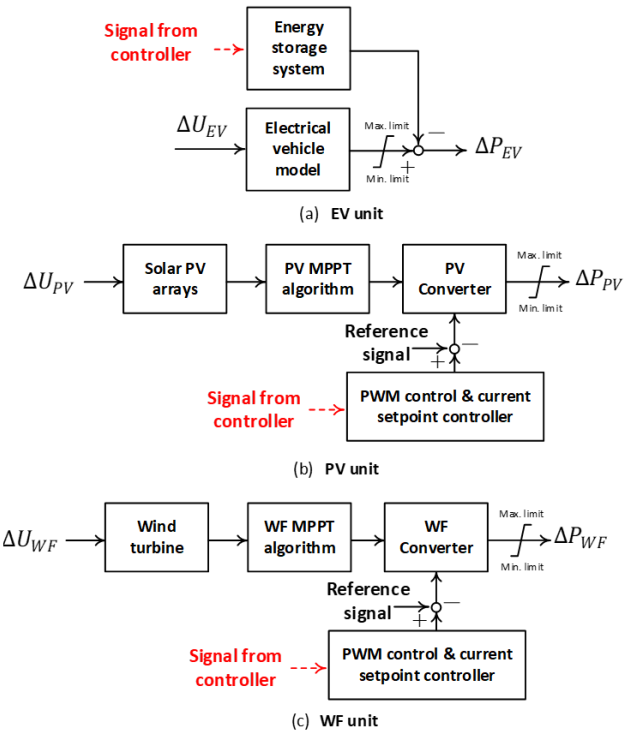

FIGURE 3. EV, PV, and WF modeling.

wave components as follows,

$$\Delta U_{PV}(s) = \bar{U}_{PV} \pm \Delta\tilde{U}_{PV}(s), \tag{7}$$

$$\Delta U_{WF}(s) = \bar{U}_{WF} \pm \Delta\tilde{U}_{WF}(s), \tag{8}$$

where $\bar{U}_{PV}$ and $\bar{U}_{WF}$ are mean values of solar radiation and wind speed, respectively, and $\Delta\tilde{U}_{PV}$ and $\tilde{U}_{WF}(s)$ are

variable parts of solar radiation and wind speed, respectively. Applying (7) and (8) to the microgrid will lead to a significant deviation in system frequency. In this article, an intermittent number of EVs charging in a day is modeled by,

$$\Delta U_{EV} = \sum_{i=1}^{N_{EV}} (L_{EV} \cdot P^{r}_{EV,i}), \tag{9}$$

where N_{EV} is the total number of EVs in the grid, L_{EV} is a logical number (0 or 1), and $P^{r}_{EV,i}$ is the rated power of the i^{th} EV. In fact, the number of EVs at the charging station varies. As a result, the variation can also affect frequency deviation in the PVs and WFs.

C. MICROGRID CONFIGURATION

The studied microgrid in Fig. 1 contains several types of generation sources with different types of load, utilized to establish the multisource nature of the microgrid. The main thermal power station has 15 MW of installed capacity, representing conventional generation using synchronous based generator. The generated electricity is consumed by a load at rated power about 55 MW. The system has 3×7 MW installed capacity for the WFs and 3×5 MW installed capacity for the PVs. In addition, EVs with a total power capacity of 30×0.1 MW are also connected to the microgrids as shown in Fig. 1. It is assumed that the energy storage system with the same size as the total EV energy is connected at the same bus to control power output of those EVs. As a result, the renewable power generation and EVs will randomly change the microgrid operating point, affecting system frequency stability and performance. It should be noted that the system base is 20 MW.

Fig. 2 is developed for both frequency analysis and study. To obtain the physical system dynamics, the generation rate constraint (GRC) for the governor unit, dead band for the turbine unit, and time delay for the secondary control or load frequency control (LFC) unit are contemplated which create an accurate frequency perception and nonlinearity of the microgrid. Therefore, the GRC is specified as $\approx 10\% - 15\%$ MW/min. The dead band limiter is specified as 0.06% (0.035 Hz). The local time delay is varied between 0 and 0.05 s. Three main control units (droop control, energy storage system, and converter) are applied to maintain system frequency stability during the exigency. The inertia control-based energy storage system is responsible for balancing the mismatch power at $1 - 10$ s. The primary control unit (i.e., the governor) is applied to stabilizing the system frequency to a new steady-state value within $10 - 30$ s. The converter control based on area control error is responsible for recovering the system frequency to its nominal value within $10 - 30$ minutes. However, because uncertain load demands (industrial and/or commercial and/or residential loads) do not participate in the frequency regulation, they can be regarded as disturbances to microgrid uncertainties. This is confirmed that the simplified model has high accuracy under a wide range of operating conditions. Therefore, the simplified model used in this article is accurate enough for frequency stability study and analysis. Moreover, the converter can provide very fast frequency recovery, so it can be ensured that converter control can be effectively used to stabilize frequency deviation.

Next, by considering the dynamic effects of 1) generation and loads including inertia, droop, and 2) converter control of EVs, PVs, and WFs, the system frequency deviation explained in [7], [8] is given as,

$$\Delta F(s) = \left(\frac{1}{2HsD}\right) \sum_{i=1}^{N_G} \Delta P_{m,i} - \sum_{l=1}^{N_l} \Delta P_{L,l}. \tag{10}$$

Then, we have

$$\Delta F(s) = \left(\frac{1}{2HsD}\right) \Big(\sum \Delta P_G + \sum \Delta P_{EV} + \sum \Delta P_{PV} + \sum \Delta P_{WF} \Big) - \sum_{l=1}^{N_l} \Delta P_{L,l}. \tag{11}$$

where $\{\Delta P_G, \Delta P_{EV}, \Delta P_{PV}, \Delta P_{WF}\} \in \Delta P_{m,i}$.

The state equation in the model as shown in Fig. 2 can be written as (12) and (13) which are used for testing the performance of the proposed control method as,

$$\Delta \dot{\mathbf{X}}(s) = A\Delta \mathbf{X}(s) + B\Delta \mathbf{U}(s), \tag{12}$$

$$\Delta \mathbf{Y}(s) = C\Delta \mathbf{X}(s) + D\Delta \mathbf{U}(s). \tag{13}$$

It is assumed that there is no feed forward in this system: so, $D = [\mathbf{0}]$. Substituting (4)-(6) in (12) and (13), the system including variable time delay at the input-output pair of controller is given as,

$$\Delta \dot{\mathbf{X}}(s) = A\Delta \mathbf{X}(s) + B\Delta \mathbf{U}(s) \cdot e^{\tau s}, \tag{14}$$

$$\Delta \mathbf{Y}(s) \cdot e^{\tau s} = C\Delta \mathbf{X}(s) \cdot e^{\tau s}, \tag{15}$$

where $\dot{\mathbf{X}}$ is the derivative of state the variable in the microgrid; X, U,and Y are state, input, and output vectors, respectively, and A, B, C,and D are state, input, output, and feed forward metrics, respectively. As a result, the system in Fig. 2 can be written as a closed-loop system by using the feedback gain law [25] as follows,

$$\Delta \dot{\mathbf{X}}'_{cl}(s) = (A - B\mathbf{U}(s) \cdot e^{\tau s}) \cdot \Delta \mathbf{X}_{cl}(s) \tag{16a}$$

$$= (A - B\mathbf{U}(s)P(s)) \cdot \Delta \mathbf{X}_{cl}(s) \tag{16b}$$

$$= [A\Delta \mathbf{X}_{cl}(s)] - [B'\mathbf{U}'(s) \cdot \Delta \mathbf{X}'_{cl}(s)], \tag{16c}$$

where superscript $'$ means that variable time delay is included, and $P(s)$ is the rational polynomial matrix of the variable time delay.

In this article, $\mathbf{K}(s)$ can be written in a form of output $\Delta \mathbf{Y}$ and control signals $\Delta \mathbf{U}$ by rewriting (16c) as,

$$\Delta \dot{\mathbf{X}}'_{cl}(s) = [A\Delta \mathbf{X}_{cl}(s)] - [B' \cdot C'\Delta \mathbf{X}'(s)\mathbf{K}(s) \cdot \Delta \mathbf{X}'_{cl}(s)], \tag{17}$$

where subscript cl means of the close-looped system. In can be seen that variable time delay affects the second term of (17) and can degrade the closed-loop system stability.

In this article, $K(s)$ is the adaptive PI controller consisting of proportional K_p and integral K_i, and it can be written as,

$$\mathbf{K}_k(s) = K_{p,k} + K_{i,k}s, \tag{18}$$

where subscript k denotes the k^{th} operation.

D. PROPOSED PI CONTROLLER UNDER VARIOUS OPERATIONS

In the time domain t, the fixed structure controller may not be able to regulate the system frequency under such changing operations because the operation of the system always changes. To design a PI controller under different operations, the closed-loop state equation in time domain is given by,

$$\Delta\dot{\mathbf{X}}'_{cl,k}(t) = A'_{cl,k}(t)\mathbf{X}'_{cl,k}(t), \tag{19}$$

where $A_{cl,k}$ is the closed-loop state matrix including $\mathbf{K}_k$ at any k^{th} operating points. Then, rewriting (19) in the form of elements in the matrix yields,

$$\dot{\mathbf{X}}'_{cl,k}(t) = \begin{bmatrix} a_{11,k}(t) & \cdots & a_{1m,k}(t) \\ \vdots & \ddots & \vdots \\ a_{m1,k}(t) & \cdots & a_{mm,k}(t) \end{bmatrix}_{m\times m} \times \begin{bmatrix} x_{1,cl} \pm \Delta x_{m,k}(t) \\ \vdots \\ x_{m,cl} \pm \Delta x_{1,k}(t) \end{bmatrix}_{m\times 1}, \tag{20}$$

where $a_{11,k}, \cdots, a_{mm,k}$ are the elements of $A_{cl,k}$, $x_{1,cl}$, $\cdots, x_{m,cl}$ are elements of $\mathbf{X}'_{cl,k}$ in steady state, and $\Delta x_{1,k}(t), \cdots, \Delta x_{m,k}(t)$ are small changes of the elements of $\mathbf{X}'_{cl,k}$, where subscript m is the dimension of the matrix. At the k^{th} operation, let $\dot{\mathbf{F}}'_k$ be the derivative of system frequency, $f_{1,k}, \cdots, f_{n,k}$ be state variables corresponding to frequency, and $a^f_{11,k}, \cdots, a^f_{nn,k}$ be elements of the frequency matrix, where $\dot{\mathbf{F}}'_k \in \mathbf{X}'_{cl,k}$ and $n < m$. Extracting (20) by focusing only on frequency, we have,

$$\begin{bmatrix} \dot{f}_{1,k}(t) \\ \vdots \\ \dot{f}_{1,k}(t) \end{bmatrix} = \begin{bmatrix} a^f_{11,k} & \cdots & a^f_{1n,k} \\ \vdots & \ddots & \vdots \\ a^f_{n1,k} & \cdots & a^f_{1n,k} \end{bmatrix}_{n\times n} \times \begin{bmatrix} f \pm \Delta f_{1,k}(t) \\ \vdots \\ f \pm \Delta f_{n,k}(t) \end{bmatrix}. \tag{21}$$

Then, expressing (20) yields,

$$\begin{bmatrix} \dot{f}_{1,k}(t) \\ \vdots \\ \dot{f}_{1,k}(t) \end{bmatrix} = \begin{bmatrix} a^f_{11,k}(f \pm \Delta f_{1,k}(t)) + \cdots + a^f_{1n,k}(f \pm \Delta f_{n,k}(t)) \\ \vdots \\ a^f_{11,k}(f \pm \Delta f_{1,k}(t)) + \cdots + a^f_{1n,k}(f \pm \Delta f_{n,k}(t)) \end{bmatrix}_{n\times 1}. \tag{22}$$

It is obvious from (22) that, when $a^f_{11,k}, \cdots, a^f_{nn,k}$ are minimized by changing the control parameters in $\mathbf{K}_k$, the effect of frequency deviation $\Delta f_{1,k}, \ldots, \Delta f_{n,k}$ is consequently reduced. As a result, this impact can be alleviated by minimizing the following function,

$$\min \begin{Bmatrix} \left|a^f_{11,k}\right| \cdots \left|a^f_{1n,k}\right| \\ \vdots \\ \left|a^f_{n1,k}\right| \cdots \left|a^f_{nn,k}\right| \end{Bmatrix}, \tag{23}$$

$$\text{Subject to} \quad 0.95f < f < 1.05f, \tag{24}$$

where min means the minimum value and $|\cdot|$ denotes the absolute value.

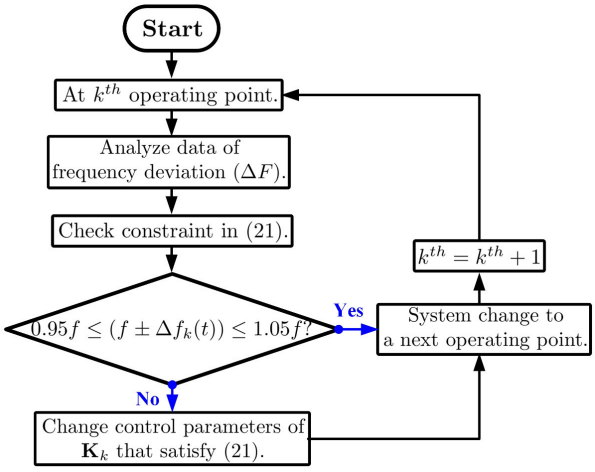

FIGURE 4. Flowchart of the proposed control strategy.

E. PROPOSED ADAPTIVE CONTROL ALGORITHM

The proposed adaptive control algorithm is applied to change the control parameters of $\mathbf{K}_k$ to guarantee the minimum value of (23) under constraints (24) under all operations. Fig. 4 demonstrates the proposed adaptive control algorithm. It can be described by the following steps:

e.i) At any k^{th} operation, we can analyze the frequency deviation data $\Delta\mathbf{F}$,

e.ii) Next, we can check constraint (24);
If $0.95f < (f \pm \Delta f_k(t)) < 1.05f$, find optimal control parameters $\mathbf{K}_{p,k}$ and $\mathbf{K}_{i,k}$ that satisfy (23);
Otherwise, the system is changed to the next operation: $k^{th} = (k+1)^{th}$,

e.iii) At the next $k^{th} = (k+1)^{th}$ generation, we can reconsider the system by going to step *e*.i). and recheck constraint (24) by going to step *e*.ii).

By repeatedly conducting steps *e*.i) - *e*.iii), the value of (23) is consequently minimized at all operating points. Consequently, oscillations of frequency under all operations are suppressed. Note that, the optimization problem of (23) is solved by using the particle swarm algorithm [26], [27].

The superiority of the proposed adaptive controller over conventional fixed controllers are given as follows:

i) The proposed adaptive controller can automatically adapt their control parameters to satisfy the objective function (23) under the constraint (24). As a result,

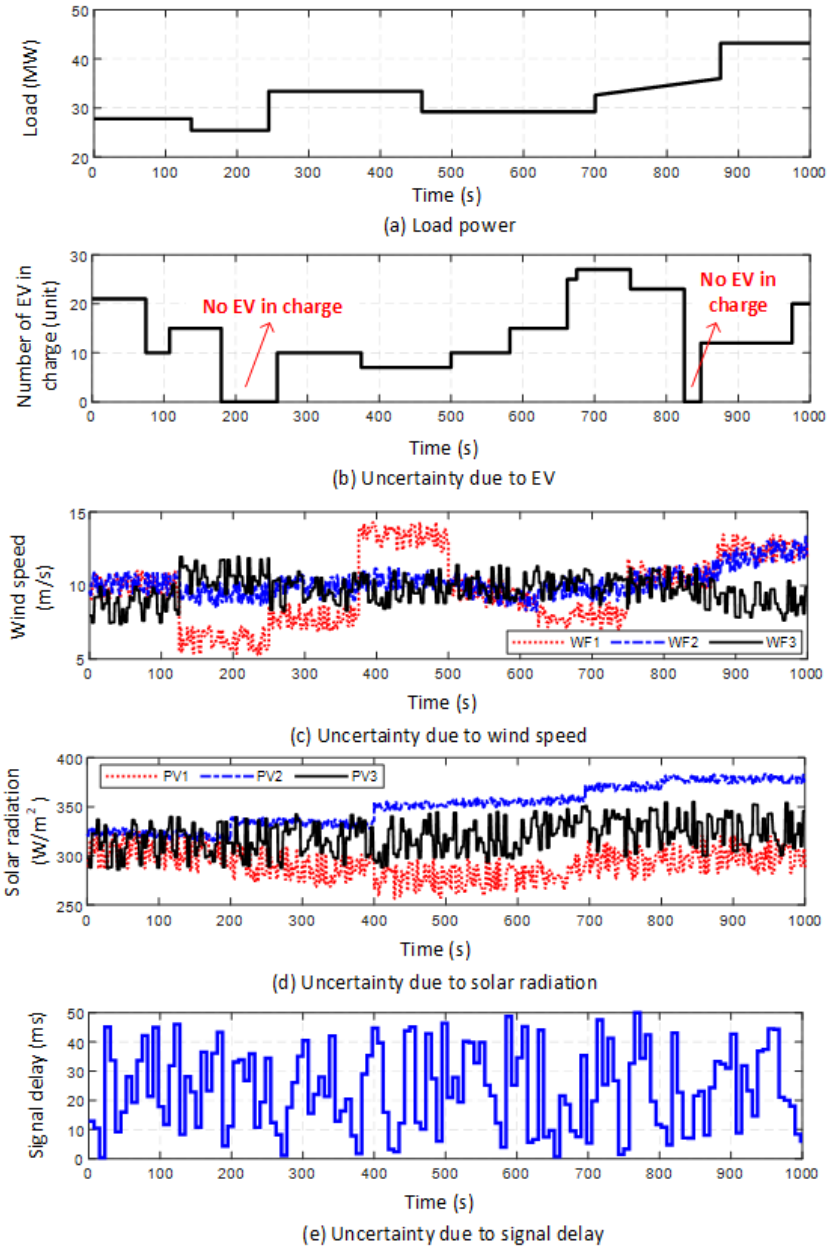

FIGURE 5. Patterns of load, number of EVs charging, wind speed, solar radiation, and signal delay.

the frequency fluctuation can be suppressed in a wind range of system operating points,

ii) Since the optimization is conducted in frequency domain using only data of frequency deviation in the system, the fast computational time can be guaranteed. As a result, the proposed method is suitable for a real time application.

IV. RESULT AND DISCUSSION

Simulation results of the case study in this section were conducted by using MATLAB and Simulink with the Control System Toolbox [28], Signal Processing Toolbox [29], and Optimization Toolbox [30]. The system parameters in Fig. 2 used as the study system are given in Table 1. In this study, the proposed controller, designed by using objective function (23) based on the adaptive algorithm in Fig. 4, is recognized as the *proposed adaptive PI controller*. To verify the performance of the proposed method, the *proposed adaptive PI controller* is compared with the conventional fixed PI controller (known as the *fixed PI controller*) under various uncertainties and disturbances. To demonstrate the superiority of the adaptive algorithm, the *fixed PI controller* is designed by using objective function (23) at the normal operating point $t = 0$s.

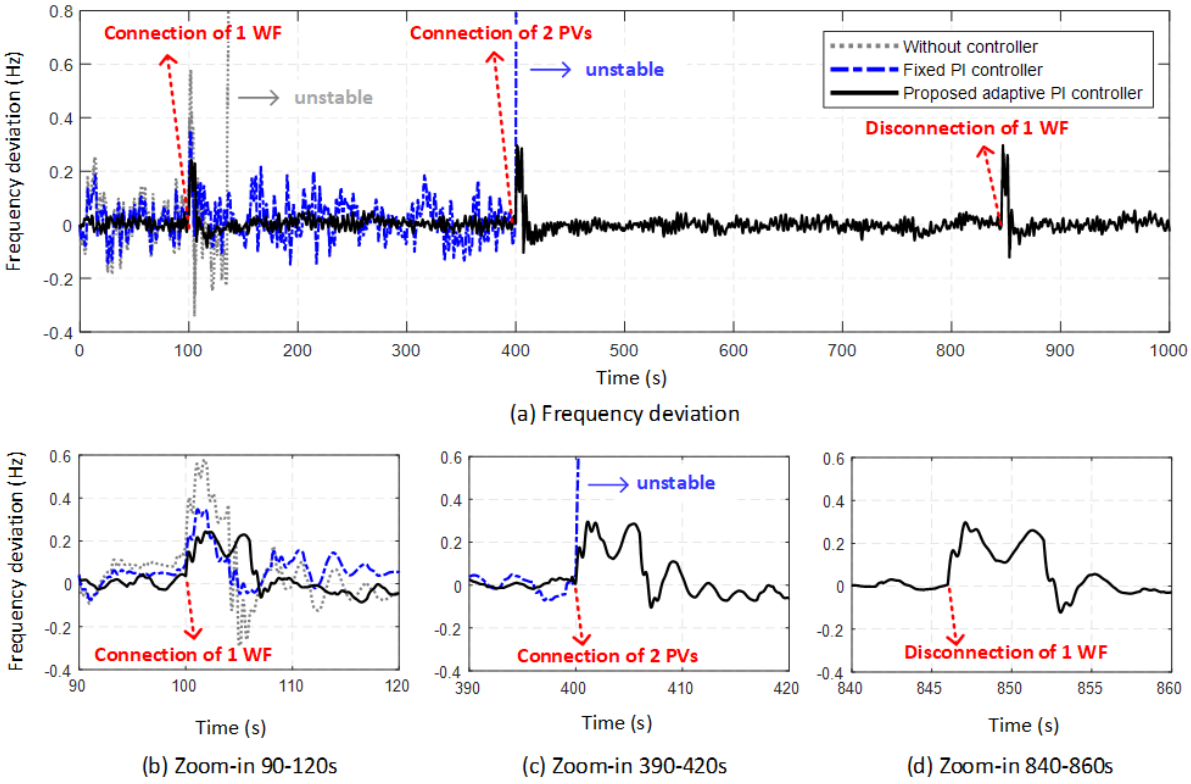

FIGURE 6. Frequency deviation under the effect of continuous uncertainties and disturbances.

TABLE 1. System parameters (system base of 50 Hz and 20 MW).

Parameter	Value
Damping coefficient, D	0.02 pu
Inertia constant, H	0.080 pu
Governor time constant, T_g	0.12 s
Turbine constant, T_b	0.43 s
Droop, R	1.75
Maximum limit of PI controller	+0.2 pu
Minimum limit of PI controller	-0.2 pu

Then, the transient simulation was conducted. Fig. 5. shows patterns of load, number of EVs charging, wind speed, solar radiation, and signal delay used in the simulation study. Fig. 5(a) illustrates the changes in load between 25 and 45MW during the simulation time. Fig. 5(b) depicts the pattern of the number of EVs charging. It can be seen that the number of EVs varies according to the time frame. During 180-350s and 820-840s, it is assumed that there are no EVs at the charging station. During these periods, the EVs are unavailable and cannot be used to stabilize the frequency fluctuation. As shown in Fig. 5(c), the WFs are simulated under variable wind speeds between 6 and 15 m/s. Here, the wind gust effect (abrupt variance from ≈5 to ≈15 m/s) is also applied to WF1 during 120 – 500 s. In the same way, in Fig. 5(d), the solar radiation of the three PVs is varied between 250 and 375 W/m^2. Also, the impact of signal delay in Fig. 5(e) is also considered in all input–output pairs of both the *proposed adaptive PI controller* and the *fixed PI controller*.

Fig. 6(a) illustrates the frequency deviation under the effect of such continuous uncertainties and disturbances described as follows: At $t = 0$s, during a light load, only two WFs and 1 PV are connected to the supply power of the microgrid. During $0-100$s, the proposed adaptive PI controller exhibits a better stabilizing effect in suppressing frequency deviation while the stabilizing effect of the *fixed PI controller* is slightly better than that without the controller. At $t = 100$s, one WF is connected to the microgrid. In the case without a controller, the peak of frequency deviation under the effect of this disturbance is vanished beyond 0.5 pu (or $> 5\%$ from the normal value). Conversely, in the case of the *proposed adaptive PI controller* and *fixed PI controller*, these controllers can keep the frequency deviation within an acceptable range (within $\pm 5\%$ of the normal value). An enlarged section of this state is given in Fig. 6(b).

During $100-400$s, it can be clearly observed that, at around $t = 120$s, the microgrid becomes unstable without a controller. Moreover, the *proposed adaptive PI controller* provides a significantly superior stabilizing effect compared to that of the fixed PI controller. At $t = 400$s, the load increases and two PVs are connected to supply the power to this inflated load. Accordingly, the *fixed PI controller* cannot resist this change, and the system becomes completely unstable. In contrast, the *proposed adaptive PI controller* can robustly

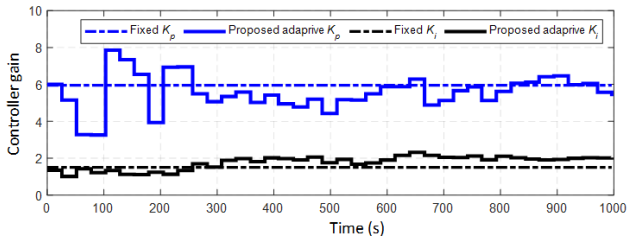

FIGURE 7. Control parameters under the effect of continuous uncertainties and disturbances.

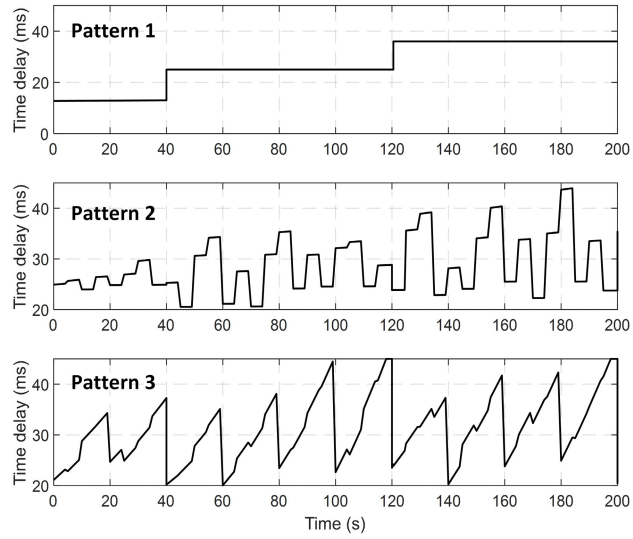

FIGURE 8. Different patterns of time delay.

maintain the frequency deviation within a stable region. Fig. 6(c) depicts an enlarged section in this period.

During $t = 400 - 1000$ s, similarly, the proposed adaptive PI controller is able to maintain frequency in the acceptable range regardless of the disconnection of the WF. Fig. 6(c) illustrates an enlarged section in this period.

Fig. 7 shows control parameters of the proposed adaptive PI controller under the effect of continuous uncertainties and disturbances. Evidently, by applying the adaptive algorithm proposed, the gains are adaptive under changing operation to maintain a minimal value of (23); therefore, the proposed controller can robustly regulate the frequency deviation of the microgrid.

Besides, the robustness of the *proposed adaptive PI controller*, validated with various time delay scenarios is investigated. Scenarios of load patterns, number of EVs charging status, wind speed, and solar radiation as shown in Fig. 5 are used in this study when the simulation time is set at 200s. Fig. 8 shows the different patterns of time delay used in this study. In Fig. 8, pattern 1 is constant time delay increasing with time domain. Patterns 2 and 3 are realistic delays of wide-area measurement system as analyzed in [31]. Note that fixed delay is set at 25ms. Accordingly, Fig. 9 demonstrates the impacts of different patterns of time delay on the *proposed adaptive PI controller* and *fixed PI controller*.

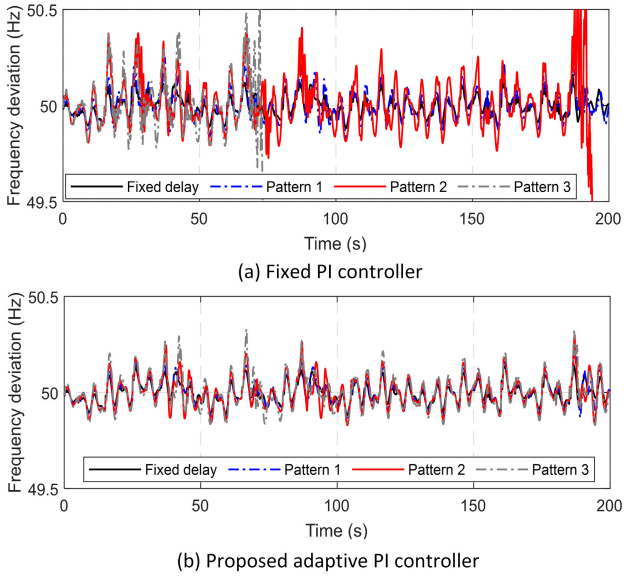

FIGURE 9. Impact of different patterns of time delay.

In comparison, the *fixed PI controller* cannot resist realistic time delay effects; more specially in time delay pattern 3 as depicted in Fig. 9 (a): this leads to system instability. On the other hand, the *proposed adaptive PI controller* can robustly handle adverse effects of all delay patterns as shown in Fig. 9 (b).

V. CONCLUSION

The coordinated control of EVs and WF and PV generation of a microgrid for microgrid frequency regulation has been proposed in this article. The significant findings are given as follows:

i) Mathematical analysis of microgrid system including WFs, PVs and EVs is given. Moreover, effect of time delay and continuous disturbance is investigated,
ii) Significant improvement in frequency stability can be obtained by using the proposed adaptive PI controller under disconnection and connection of renewable energy sources,
iii) By applying the proposed algorithm, the proposed controller can adaptively change the control parameters according to system operations including dynamic models of WF, PV, and EVs,
iv) Superior stabilizing effects of the proposed adaptive PI controller over a conventional fixed PI controller can be achieved under continuous system uncertainties, disturbances, and various patterns of realistic time delay.

According to the obtained results, it is promising that the proposed adaptive coordinated controller can be applied in a microgrid, consisting of WF, PV and EVs. Also, the developed adaptive controller can be an alternative control solution for supporting the use of renewable energy sources in microgrids.

REFERENCES

[1] A. Rabiee, A. Soroudi, B. Mohammadi-ivatloo, and M. Parniani, "Corrective voltage control scheme considering demand response and stochastic wind power," *IEEE Trans. Power Syst.*, vol. 29, no. 6, pp. 2965–2973, Nov. 2014.
[2] U. Munz, A. Mesanovic, M. Metzger, and P. Wolfrum, "Robust optimal dispatch, secondary, and primary reserve allocation for power systems with uncertain load and generation," *IEEE Trans. Control Syst. Technol.*, vol. 26, no. 2, pp. 475–485, Mar. 2018.
[3] R. Doherty and M. O'Malley, "A new approach to quantify reserve demand in systems with significant installed wind capacity," *IEEE Trans. Power Syst.*, vol. 20, no. 2, pp. 587–595, May 2005.
[4] K. Rahbar, C. C. Chai, and R. Zhang, "Energy cooperation optimization in microgrids with renewable energy integration," *IEEE Trans. Smart Grid*, vol. 9, no. 2, pp. 1482–1493, Mar. 2018.
[5] Y. Zhang, N. Gatsis, and G. B. Giannakis, "Robust energy management for microgrids with high-penetration renewables," *IEEE Trans. Sustain. Energy*, vol. 4, no. 4, pp. 944–953, Oct. 2013.
[6] B. Jie, T. Tsuji, and K. Uchida, "Analysis and modelling regarding frequency regulation of power systems and power supply–demand-control based on penetration of renewable energy sources," *J. Eng.*, vol. 2017, no. 13, pp. 1824–1828, 2017.
[7] T. Kerdphol, F. S. Rahman, Y. Mitani, M. Watanabe, and S. Kufeoglu, "Robust virtual inertia control of an islanded microgrid considering high penetration of renewable energy," *IEEE Access*, vol. 6, pp. 625–636, 2018.
[8] T. Kerdphol, F. S. Rahman, M. Watanabe, Y. Mitani, D. Turschner, and H.-P. Beck, "Enhanced virtual inertia control based on derivative technique to emulate simultaneous inertia and damping properties for microgrid frequency regulation," *IEEE Access*, vol. 7, pp. 14422–14433, 2019.
[9] S. Liu, X. Wang, and P. X. Liu, "Impact of communication delays on secondary frequency control in an islanded microgrid," *IEEE Trans. Ind. Electron.*, vol. 62, no. 4, pp. 2021–2031, Apr. 2015.
[10] A. Fathi, Q. Shafiee, and H. Bevrani, "Robust frequency control of microgrids using an extended virtual synchronous generator," *IEEE Trans. Power Syst.*, vol. 33, no. 6, pp. 6289–6297, Nov. 2018.
[11] G. Magdy, G. Shabib, A. A. Elbaset, T. Kerdphol, Y. Qudaih, H. Bevrani, and Y. Mitani, "Tustin's technique based digital decentralized load frequency control in a realistic multi power system considering wind farms and communications delays," *Ain Shams Eng. J.*, vol. 10, no. 2, pp. 327–341, Jun. 2019.
[12] X. Wu, C. Shen, and R. Iravani, "A distributed, cooperative frequency and voltage control for microgrids," *IEEE Trans. Smart Grid*, vol. 9, no. 4, pp. 2764–2776, Jul. 2018.
[13] H. Li, X. Wang, and J. Xiao, "Adaptive event-triggered load frequency control for interconnected microgrids by observer-based sliding mode control," *IEEE Access*, vol. 7, pp. 68271–68280, 2019.
[14] J. Zhao, X. Lyu, Y. Fu, X. Hu, and F. Li, "Coordinated microgrid frequency regulation based on DFIG variable coefficient using virtual inertia and primary frequency control," *IEEE Trans. Energy Convers.*, vol. 31, no. 3, pp. 833–845, Sep. 2016.
[15] H. Ali, G. Magdy, B. Li, G. Shabib, A. A. Elbaset, D. Xu, and Y. Mitani, "A new frequency control strategy in an islanded microgrid using virtual inertia control-based coefficient diagram method," *IEEE Access*, vol. 7, pp. 16979–16990, 2019.
[16] A. Latif, D. C. Das, S. Ranjan, and A. K. Barik, "Comparative performance evaluation of WCA-optimised non-integer controller employed with WPG–DSPG–PHEV based isolated two-area interconnected microgrid system," *IET Renew. Power Gener.*, vol. 13, no. 5, pp. 725–736, 2019.
[17] S. Ranjan, D. C. Das, A. Latif, and N. Sinha, "LFC for autonomous hybrid micro grid system of 3 unequal renewable areas using mine blast algorithm," *Int. J. Renew. Energy Res. (IJRER)*, vol. 8, no. 3, pp. 1297–1308, 2018.
[18] A. Latif, D. C. Das, A. K. Barik, and S. Ranjan, "Maiden coordinated load frequency control strategy for ST-AWEC-GEC-BDDG-based independent three-area interconnected microgrid system with the combined effect of diverse energy storage and DC link using BOA-optimised PFOID controller," *IET Renew. Power Gener.*, vol. 13, no. 14, pp. 2634–2646, Oct. 2019.
[19] A. Latif, D. C. Das, A. K. Barik, and S. Ranjan, "Illustration of demand response supported co-ordinated system performance evaluation of YSGA optimized dual stage PIFOD-(1+PI) controller employed with wind-tidal-biodiesel based independent two-area interconnected microgrid system," *IET Renew. Power Gener.*, vol. 14, no. 6, pp. 1074–1086, Apr. 2020.
[20] A. Latif, S. M. S. Hussain, D. C. Das, and T. S. Ustun, "State-of-the-art of controllers and soft computing techniques for regulated load frequency management of single/multi-area traditional and renewable energy based power systems," *Appl. Energy*, vol. 266, May 2020, Art. no. 114858.
[21] Z. Zhao, P. Yang, J. M. Guerrero, Z. Xu, and T. C. Green, "Multiple-Time-Scales hierarchical frequency stability control strategy of medium-voltage isolated microgrid," *IEEE Trans. Power Electron.*, vol. 31, no. 8, pp. 5974–5991, Aug. 2016.
[22] P. M. Anderson and A. A. Fouad, *Power System Control and Stability*. Hoboken, NJ, USA: Wiley, 2008.
[23] B. P. Padhy, S. C. Srivastava, and N. K. Verma, "A wide-area damping controller considering network input and output delays and packet drop," *IEEE Trans. Power Syst.*, vol. 32, no. 1, pp. 166–176, Jan. 2017.
[24] L. D. Philipp, A. Mahmood, and B. L. Philipp, "An improved refinable rational approximation to the ideal time delay," *IEEE Trans. Circuits Syst. I, Fundam. Theory Appl.*, vol. 46, no. 5, pp. 637–640, May 1999.
[25] I. Nagrath, *Control Systems Engineering*. Daryaganj, New Delhi: New Age International, 2006.
[26] C.-H. Liu and Y.-Y. Hsu, "Design of a self-tuning PI controller for a STATCOM using particle swarm optimization," *IEEE Trans. Ind. Electron.*, vol. 57, no. 2, pp. 702–715, Feb. 2010.
[27] C.-F. Juang and C.-F. Lu, "Load-frequency control by hybrid evolutionary fuzzy PI controller," *IEE Proc.-Gener. Transmiss. Distrib.*, vol. 153, no. 2, pp. 196–204, 2006.
[28] D. K. Frederick and J. Chow, *Feedback Control Problems Using MATLAB and the Control System Toolbox*. Seattle, WA, USA: Brooks/Cole Publishing, 1999.
[29] T. P. Krauss, L. Shure, and J. Little, *Signal Processing Toolbox for Use With MATLAB: User's Guide*. Natick, MA, USA: MathWorks, 1994.
[30] T. Coleman, M. A. Branch, and A. Grace, "Optimization toolbox," in *For Use With MATLAB. User's Guide for MATLAB Version 2, Relaese II*, vol. 5. Natick, MA, USA: MathWorks, 1999.
[31] M. Liu, I. Dassios, G. Tzounas, and F. Milano, "Stability analysis of power systems with inclusion of realistic-modeling WAMS delays," *IEEE Trans. Power Syst.*, vol. 34, no. 1, pp. 627–636, Jan. 2019.

PHOOMPAT JAMPEETHONG (Member, IEEE) received the B.Eng. and M.Eng. degrees in electrical engineering from the King Mongkut's Institute of Technology Ladkrabang, Bangkok, Thailand, in 2003 and 2007, respectively, where he is currently pursuing the D.Eng. degree in electrical engineering. His research interests include alternative energy, electric vehicle, battery energy storage systems, and power electronics.

SURIN KHOMFOI (Senior Member, IEEE) was born in Thailand. He received the B.Eng. and M.Eng. degrees in electrical engineering from the King Mongkut's Institute of Technology Ladkrabang (KMITL), Bangkok, Thailand, in 1996 and 2000, respectively, and the Ph.D. degree in electrical engineering from The University of Tennessee, Knoxville, TN, USA, in 2007.

Since December 1997, he has been a Lecturer with the Department of Electrical Engineering, KMITL, where he is currently an Associate Professor. His current research interests include multi-level power converters, renewable energy applications, fault diagnosis, power quality, and smart grids. He is a member of the Eta Kappa Nu Honor Society. He was a recipient of the Academic Scholarship Awards, including the Full Academic Scholarship for his B.Eng., M.Eng., and Ph.D. studies from the Energy Policy and Planning Office (EPPO), Ministry of Energy, Thailand.